

Engineering local optimality in Quantum Monte Carlo algorithms

Lode Pollet,^{*} Kris Van Houcke, and Stefan M. A. Rombouts

Vakgroep subatomaire en stralingsfysica,

Proeftuinstraat 86,

Universiteit Gent, Belgium

(Dated: December 2, 2024)

Quantum Monte Carlo algorithms based on a world-line representation such as the worm algorithm and the directed loop algorithm are among the most powerful numerical techniques for the simulation of non-frustrated spin models and of bosonic models. Both algorithms work in the grand-canonical ensemble and have a non-zero winding number. However, they retain a lot of intrinsic degrees of freedom which can be used to optimize the algorithm. We let us guide by the rigorous statements on the globally optimal form of Markov chain Monte Carlo simulations in order to devise a locally optimal formulation of the worm algorithm while incorporating ideas from the directed loop algorithm. We provide numerical examples for the soft-core Bose-Hubbard model and various spin- S models.

PACS numbers: 02.70.Tt, 05.50.+q, 82.20.Wt

I. INTRODUCTION

Monte Carlo methods have become a standard numerical tool in many branches of science, offering exact results in a statistical sense [1]. In physics, Monte Carlo algorithms still resemble the original description by Metropolis [2] in the fifties, but computational physicists have elaborated them. For instance, Ising and other lattice models constituted one of the key initial problems of interest to the emerging Monte Carlo community, but the slowing down in the neighborhood of the second order phase transition has only recently been overcome by cluster updates [3, 4]. These algorithms are still in the same spirit as the Metropolis scheme. Monte Carlo methods have also been applied to quantum many-body systems, where one tries to sample either the wavefunction or the partition function [5]. The quantum analog of cluster updates, namely the loop algorithm [6], triggered the development of the worm algorithm [7] and the operator loop algorithm [8] (and later the directed loop algorithm [9, 10]) in the stochastic series expansion representation. These algorithms share the properties that they sample the one-body Green function, that they are formulated in continuous time [11] and are based on a world-line representation. Thus both algorithms are similar and they differ in fact only by the chosen representation [12]. These algorithms have successfully been applied to spin systems and to the Bose-Hubbard model [13]. Recently, the worm algorithm has been formulated in the canonical ensemble, allowing to study more systems including superconducting grains and the nuclear pairing Hamiltonian [14, 15].

The efficiency of a numerical simulation method is primordial: efficient algorithms lead to more accurate

results at the same computational cost and allow for the study of larger systems. The algorithms mentioned above are based on a Markov process that results in a random walk in a specific configuration space. Configurations are visited by the random walker proportionally to their respective weights. By the Markov process, subsequent measurements are trivially correlated. The transition matrix specifies the probability of going from one configuration to another, and has to be defined in advance. In practice, one requires that transition matrices satisfy the principle of detailed balance [1]. This, however, still leaves some freedom in the choice of the transition matrices, which can be used to optimize the efficiency of the algorithm. A convenient updating scheme is the Metropolis-Hastings algorithm [2, 16]: a limited number of configurations can be reached from the current one by defining a proposal distribution, and the transition to the new configuration is accepted or rejected according to detailed balance [1].

In previous work, we introduced the notion of 'locally optimal Monte Carlo' [17], when the degrees of freedom of every transition matrix are chosen in such a way as to mimic the globally optimal transition matrix, which, at least in principle, can be written down exactly. This approach is a best guess for obtaining optimal efficiency, and was found successful in practice for the directed loop algorithm in the stochastic series expansion representation [17]. Here we investigate the consequences of the locally optimal Monte Carlo idea for the worm algorithm, and try to combine the advantages of the directed loop algorithm with the advantages of the worm algorithm. This results in a new formulation of the worm algorithm, hereafter called the locally optimal worm algorithm (LOWA) [18]. We show results for various spin models and the Bose-Hubbard model, and compare the efficiency of the LOWA with that of the directed loop algorithm in the stochastic series expansion framework.

^{*}Electronic address: Lode.Pollet@UGent.be

II. THE ALGORITHM

We consider a two-body Hamiltonian H defined on a discrete lattice which can be written as $H = H_0 - V$, where the terms H_0 and V are to be specified later on. We also assume a single particle basis $|i_\nu\rangle$ of H_0 such that the action of any term in the Hamiltonian on a basis state yields a new basis state. The models that we typically have in mind are the Bose-Hubbard model,

$$H = -t \sum_{\langle i,j \rangle} b_i^\dagger b_j + \frac{U}{2} \sum_i n_i(n_i - 1) + V_{nn} \sum_{\langle i,j \rangle} n_i n_j - \sum_i \mu n_i \quad (1)$$

and a general spin- S model,

$$H = J \sum_{\langle i,j \rangle} \frac{1}{2} (S_i^+ S_j^- + S_i^- S_j^+) + \Delta S_i^z S_j^z - h \sum_i S_i^z, \quad (2)$$

In both expressions the notation $\langle i, j \rangle$ refers to the sum over nearest-neighbor sites only. In the Bose-Hubbard model, bosons are created on site j by the operator b_j^\dagger and the number of bosons on site j is counted by the number operator n_j . The kinetic term describes hopping of the bosons with tunneling amplitude t , while we consider two kinds of potential energy : on-site repulsion with strength U and nearest-neighbor repulsion with strength V_{nn} . For the spin anti-ferromagnet (spin exchange amplitude $J > 0$), we require that the lattice is bipartite. All matrix elements remain positive as long as the model does not exhibit any frustration which can for instance be induced by second nearest-neighbor hopping. As the calculations serve to demonstrate the ideas related to efficiency, we restrict the discussion to one dimension.

A worm algorithm [7] is a quantum Monte Carlo algorithm where the decomposition of the partition function,

$$Z = \sum_{n=0}^{\infty} \int_0^\beta dt_n \int_0^{t_n} dt_{n-1} \cdots \int_0^{t_2} dt_1 \quad (3)$$

$$e^{-t_1 H_0} V e^{-(t_2 - t_1) H_0} \dots e^{-(t_n - t_{n-1}) H_0} V e^{-(\beta - t_n) H_0},$$

is embedded in the extended configuration space

$$Z_e[U(i, j, \tau)] = \text{Tr} \left[\mathcal{T} \left(\left(b_i(0) b_j^\dagger(\tau) + \text{h.c.} \right) \exp(-\beta H) \right) \right]. \quad (4)$$

The symbol \mathcal{T} denotes time ordering, and we have introduced the Heisenberg operators $(b_i(0) b_j^\dagger(\tau) + b_i^\dagger(0) b_j(\tau))$ which we call the 'worm' operators. The worm consists of a stationary (denoted by the symbol (0)) tail at a random point in space-time, and a mobile head which can propagate in imaginary time and over the lattice. The choice $H_0 = 0, V = -H$

allows one to integrate over all times in the partition function, and leads to the stochastic series expansion representation. The worm algorithm on the other hand is obtained by collecting all diagonal one-body and diagonal two-body terms into H_0 (with respect to a chosen basis), while the off-diagonal one-body operators are put in V . Updates sample the Green function and are local in the extended configuration space. The directed loop algorithm is thus a special case of the worm algorithm, they merely differ by the representation [12]. In this paper we think about a new formulation for the worm algorithm that incorporates the ideas of locally optimal Monte Carlo.

Compared to the original formulation of the worm algorithm by Prokofev *et al.* [7], the efficiency of the directed loop algorithm in the stochastic series expansion representation was found superior for spin systems and even for a homogeneous Bose-Hubbard model in both phases (except for the extreme soft-core case) [19]. This is an expected result for spin systems where the diagonal energies are of the same order as the spin exchange amplitudes, but for the Bose-Hubbard model this result feels unsatisfactory. For a trapped Bose-Hubbard model however, the worm algorithm was found superior [19].

The origins of the efficiency of the directed loop algorithm [9, 10] in the stochastic series expansion framework are various:

- When directed loops are applied, the direction of the worm propagation does not randomly alter after the worm has passed an interaction. This ensures large changes in configuration space along the imaginary time axis.
- the concept of 'locally optimal Monte Carlo' is very powerful in the determination of how a worm has to pass (and modify) an interaction. This enhances changes along the spatial directions.
- Integrating over the imaginary times from the onset allows for a very efficient implementation with only integer number operations when the stochastic series expansion representation is used. The doubly linked list can be implemented by compiler optimized data structures. The down side of this approach is that a separate diagonal update is needed and that the construction of the doubly linked list involves a copy operation.

With these observations as guidelines, we are looking for a worm algorithm with properties that are a combination of the best of both approaches:

- the worm has the ability to insert, pass or annihilate interactions. Detailed balance should be imposed between these processes using the concept of locally optimal Monte Carlo [17].

- due to the exponential factors representing the diagonal weights in eq.(3), imaginary time jumps by the worm are sampled using the exponential distribution. Compared to previous implementations of the worm algorithm [7, 13], we do not consider time intervals of constant energy, nor will we insert and annihilate interactions by jump/anti-jump processes.
- The worm is tagged by an extra label 'direction'. This label is dummy, as it does not appear in eq.(3). In addition, worms can be raising or lowering. The direction of propagation can only change when the worm encounters an interaction.

We describe now the algorithm which has the above mentioned features. We have the Bose-Hubbard model in mind; the description of the algorithm for spin systems is analogous.

1. Pick an arbitrary site and an arbitrary time and call it (i_0, τ_0) . Find the occupation on all sites at that particular time τ_0 . A direction (left or right) is chosen with equal probability. Assume propagation to the right was chosen.
2. At (i_0, τ_0) a worm-pair (tail-head) is inserted. If the occupation is higher than zero, the worm-pair can be raising or lowering with equal probability. The occupation in the infinitesimal interval between worm tail and worm head is increased by one for a lowering worm-pair. If the occupation at (i_0, τ_0) is zero, then with probability 50% a lowering worm is inserted and with probability 50% no worm is inserted. The insertion probabilities are thus the same as for the directed loop algorithm [20].
3. When moving to the right (left), we call E the energy to the left (right) of the worm head. Draw an exponential deviate, $p = -\ln(u)$ with u an uniform random number, $0 < u \leq 1$. Evaluate the imaginary time shift window $\Delta\tau = p/E$ and the new worm time $\tau' = \tau + \Delta\tau$.
4. If the worm head encounters the worm tail during this propagation, the update ends with probability one and we arrive at a new diagonal configuration.
5. If the new worm time is larger than the time to the next interaction, the new worm time only equals the time of the next interaction. The worm can either bounce back or pass, annihilate or modify the interaction along the rules of detailed balance defined below.
6. If no interaction is encountered in the imaginary time shift window, the worm shifts to its new time where an interaction is inserted. If it is not possible to insert an interaction, the worm changes its direction of propagation (bounces back).
7. Go back to step 3.

Observables can be updated in the same way as in the directed loop [9] and worm [7] algorithms. For the Green function, one updates a histogram every time the mobile worm crosses the imaginary time level τ_0 [21]. If the mobile worm resides on site j at that moment, then entry (i_0, j) of the histogram is updated with a value M^2 , with M the matrix element of the stationary worm. This is a consequence of explicitly taking the worm weights into account in the configuration weight [20].

Let us come back to the diagonal updates of step 3. We have to sample terms of the form

$$e^{-(t_n - t_{n-1})E_n} = e^{-\Delta t E_n} \quad (5)$$

For the Bose-Hubbard model, the diagonal energies exceed the off-diagonal matrix elements. The exponentials are thus responsible for the largest changes in the configuration weight. A locally optimal formulation implies thus the exact sampling of these terms using exponential deviates (Poisson process). There is some algorithmic freedom in this update however : We can generate these terms according to

$$e^{-\Delta t \epsilon_n}. \quad (6)$$

With the subscript notation L referring to the configuration to the left of the worm head and R to the configuration to the right of the worm head, we have that detailed balance is satisfied if $\epsilon_L - \epsilon_R = E_L - E_R$ with $\epsilon_L, \epsilon_R \geq 0$. The parameters ϵ replace thus the energies E in step 3. Possible choices for $\epsilon_{L,R}$ are

- (a) $\epsilon_{L,R} = E_0 + E_{L,R}$, with E_0 a global constant that renders all energies positive.
- (b) $\epsilon_{L,R} = E_{L,R} - \min[E_L, E_R]$. This quantity can be zero, meaning that the jump in imaginary time is infinite, i.e. that the next interaction is always reached. Compared to the previous approach, the diagonal energies are here of the same order of magnitude as the matrix elements of the off-diagonal operators, which enhances the sampling. However, we found that this parameter choice resulted in some anomalously long (non-closing) loops and in problems with ergodicity when these long loops are discarded.
- (c) $\epsilon_{L,R} = E_{L,R} - \min[E_L, E_R] + E_{off}$, where the energy offset E_{off} overcomes the aforementioned problems with ergodicity. It makes sense to choose $E_{off} = \langle V \rangle$ with $\langle V \rangle$ a typical matrix element of the interaction.

After the worm has passed an interaction at time t_n , we have to calculate the new energy parameters $\epsilon_{L,R}$ and consider a new time shift. This can be accomplished by either drawing a new exponential deviate (as in step 3), or by adjusting the time shift window $\Delta\tau \rightarrow \Delta\tau - (t_n - t_{n-1})\epsilon_L$ (when moving to the right).

We will now define the equations of detailed balance between inserting and annihilating an interaction. First, there are two simple cases. When the worm encounters an interaction whose sites are different from the site on which the worm head resides, the worm can pass the interaction with probability one. This is a consequence of the commutator of the worm operator and the interaction being zero [18]. Second, when a worm operator b_i^\dagger encounters an interaction $b_i^\dagger b_j$, it can pass the interaction with probability one. This is also the result of the commutator being zero [18].

The only situation deserving attention happens when inserting an interaction, as depicted in Fig. 1. For models with nearest-neighbor hopping, an interaction can only be inserted to both neighboring sites, meaning that we have to set up detailed balance between three different configurations. The configurations with an interaction inserted (diagrams (b) and (c) in Fig. 1) both have a total weight consisting of the weight of the interaction and the worm weight. The weight of the current configuration (diagram (a) in Fig. 1) consists of the worm weight and an energy contribution ϵ , resulting from the normalization of the exponential distribution. (Strictly speaking, the normalization factor is always present, but when the worm reaches an interaction, we have to integrate over all imaginary time jumps that would go beyond the interaction, hereby canceling the normalization factor.) The transition matrix is a 3×3 matrix, which has in principle three parameters free to choose. If no interaction is inserted, the worm bounces back. If an interaction is inserted, the direction of propagation can be maintained.

Similarly, when a worm b_i^\dagger reaches an interaction $b_j^\dagger b_i$ (depicted in diagram (b) in Fig. 1, where the worm approaches the interaction from the right), the worm can either bounce back (b), annihilate the interaction (a) while keeping the the same direction of propagation or 'relink' the interaction as in (c), when the worm jumps to another site and changes its direction of propagation.

When the worm head reaches the worm tail, the Monte Carlo step is finished. Global detailed balance is satisfied, since detailed balance is satisfied at every step of the update. The reverse worm can be constructed using the same numerical recipe as described above.

The algorithm described above is valid when the diagonal energies involve a single site, but also when the diagonal energies contain nearest-neighbor repulsion terms.

The LOWA shares thus features with the worm algorithm and with the directed loop algorithm, and is in essence another realization of the idea of sampling the Green function in a suitable representation, here the path integral representation. The directed loop algorithm has

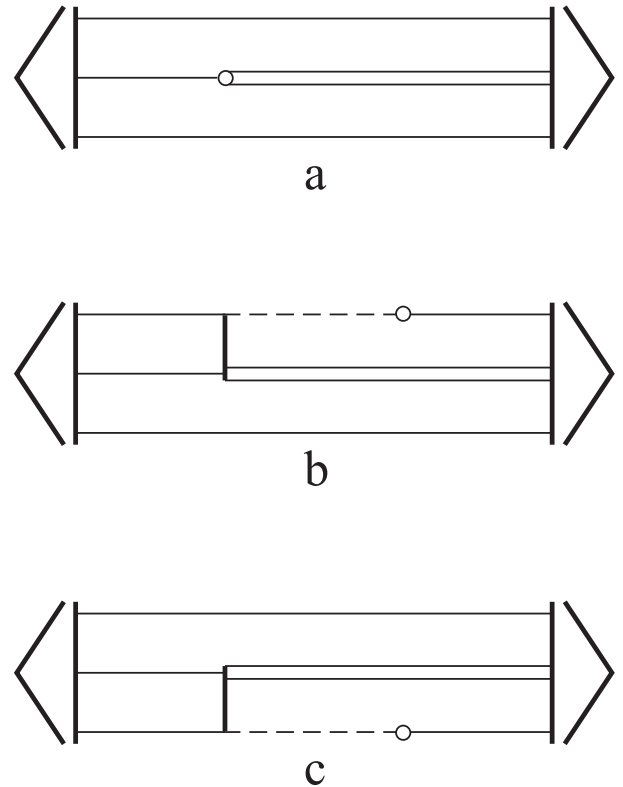


FIG. 1: When the worm moves to the right and tries to insert an interaction in configuration (a), the two possible new configurations are configurations (b) and (c). The third possibility is bouncing back and changing direction in configuration (a). The transition matrix is thus a 3×3 matrix. Interactions are denoted by a full vertical line, the mobile head of the worm by a circle. In an occupation number basis, dashed lines denote zero occupation and single/double full lines mean single/double occupation.

previously been formulated in the path integral formulation [9]. Although there are some resemblances, the LOWA is different, more general, and the principles that lie at heart of the derivation of the algorithm are different.

III. IS THE LOCALLY OPTIMAL WORM ALGORITHM EFFICIENT?

Although we have argued why we believe the proposed LOWA is efficient, we can only verify by doing numerics in order to get a definite answer on its efficiency. The results are compared with data obtained by the directed loop algorithm in the stochastic series expansion representation of Refs. [17, 20?], which will be abbreviated as DLSSE.

A direct comparison is complicated because present implementations use different data structures for both

algorithms. In the DLSSE, a doubly linked list is constructed before the loop update. Since the graph is fixed, the number of elements in this list cannot change. This allows to allocate memory statically. In the worm algorithm on the other hand, the number of interactions can change at any time. In our Fortran code this was implemented using two arrays of a predetermined fixed length, corresponding to the interactions before and after the current mobile worm time. It is possible that the performance of the worm algorithm could be different when using typical language features of e.g. C++ for the manipulation and storage of the arrays containing the interactions.

A. Bose-Hubbard model

We have calculated the standard deviations on the kinetic energy and on the squared density for a one-dimensional Bose-Hubbard model of size $L = 32$ sites at an inverse temperature of $\beta = 32$ and with a fixed chemical potential $\mu = 2$ in the absence of nearest-neighbor repulsion, $V_{nn} = 0$. We work in units $t = 1$. Simulations consisted of 40 bins that each ran 300 seconds on a Pentium III processor. We imposed a particle number cutoff of ten particles per site for $U = 1, 2$ and $U = 3$, while a cutoff of five particles per site was taken for the other values of U , ranging from $U = 4$ to $U = 10$. Imposing a cut-off is a necessity for the DLSSE, but not for the LOWA. The number of loops per update was optimized along the guidelines of Ref. [20]. The Mott phase is reached for $U = 6$.

We have calculated the standard deviation on the kinetic energy and on the density squared (i) for the DLSSE. (ii) for the LOWA where the diagonal energy parameters were chosen according to approach (a) (iii) for the LOWA where the diagonal energy parameters were chosen according to approach (c). In (ii) and (iii) the 3×3 transition matrices were taken as the locally optimal ones as in eq.(8). We shall discuss this in section III C. In Figs. 2 and 3 the results for algorithms (i) and (iii) are shown.

Among the different LOWA optimization parameters, approach (iii) is almost always the most efficient one. The DLSSE seems to be the preferred model for very low values of U . However, approach (ii) performs lots better than approach (iii) in this regime, and its efficiency is comparable to that of the DLSSE. When the diagonal matrix elements are much larger than the off-diagonal ones, as in the Mott phase $U > 6$, the present algorithm is superior. Admittedly, we recognize that it is not unambiguous how the directed loop simulations should be performed in the Mott phase because of the very short loop sizes.

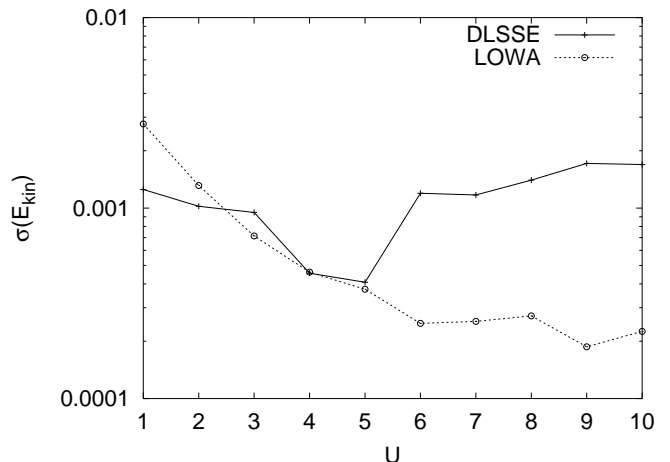


FIG. 2: Standard deviation (statistical error) on the kinetic energy for the directed loop algorithm in the stochastic series expansion framework (DLSSE), and the locally optimal worm (LOWA) using an energy offset added to the energy difference for the diagonal energy parameters and using locally optimal updates (eq.(8)). Simulations consisted of 40 bins that each ran 300 seconds on a Pentium III processor for a one-dimensional Bose-Hubbard model of $L = 32$ sites at an inverse temperature of $\beta = 32$ and with a fixed chemical potential $\mu = 2$. The accuracy of the data points is about ten percent.

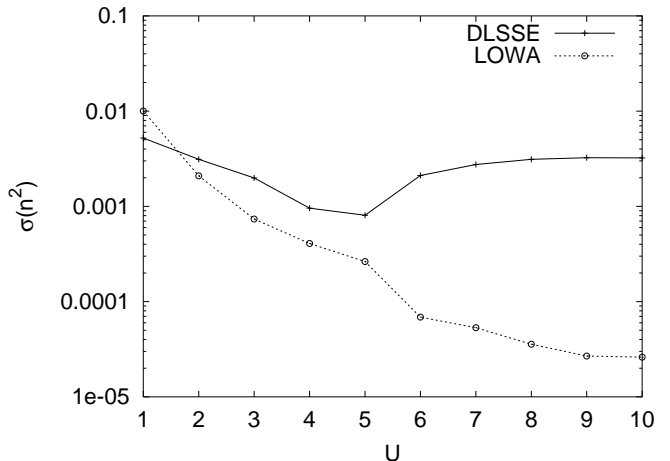


FIG. 3: Idem as in Fig. 2, but now for the standard deviation on the average square density, $\langle n^2 \rangle = \langle (\sum_i n_i)^2 \rangle / L$.

B. Spin systems

For spin systems, the magnitude of the diagonal and the off-diagonal matrix elements is of the same order. One can thus expect that the DLSSE is more efficient for spin models than for soft-core bosonic models, since diagonal and off-diagonal operators are treated on equal footing in the stochastic series expansion representation.

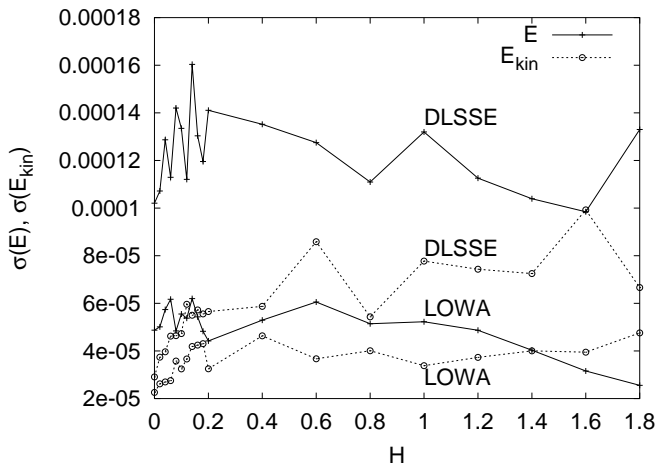


FIG. 4: Standard deviations on the total energy ($\sigma(E)$) and on the kinetic energy ($\sigma(E_{kin})$) obtained after a simulation of a spin-1/2 chain with $J = \Delta = 1$ consisting of $L = 64$ sites and with inverse temperature $\beta = 16$. Simulations have been performed with the directed loop algorithm in the stochastic series expansion framework (DLSSE) and with the locally optimal worm algorithm (LOWA). Computations consisted of 40 bins that each ran for 60 seconds on a Pentium-III processor.

It is thus interesting to compare the efficiency of the locally optimal worm with the efficiency of the DLSSE for a spin-1/2 chain. The LOWA was most efficient when the energy offset parameter was set to $E_{off} = 0.5$. In Fig. 4 the standard deviations of the total energy and of the kinetic energy are shown, which are obtained by applying the LOWA and the DLSSE to a spin-1/2 chain subject to a magnetic field H . We find that the locally optimal worm is superior to the DLSSE in our implementations, but it is more meaningful to say that both algorithms behave similarly as the magnetic field is increased, while the algorithms are most efficient near $H = 0$. Analogous conclusions were found for a spin-1 chain. For a spin-2 chain however, the DLSSE was found to be superior.

C. Heat bath updates and the locally optimal matrix

In the LOWA the transition probability matrices T have dimension three. All probabilities have to be smaller than one, while the sum of the rows in the transition probability matrix equals unity. Detailed balance requires that $W_i T_{ij} = W_j T_{ji}$, in which W_i is the weight of configuration i . Despite these requirements, there is still some algorithmic freedom left in the definition of the transition probability matrices T (in fact, three elements of the matrix T can be chosen). We will compare the numerical efficiency of two different approaches. Let us therefore order [22] and normalize the weights such that $\pi_1 \leq \pi_2 \leq \pi_3$, with $\pi_j = \frac{W_j}{\sum_k W_k}$. The heat-bath

approach T^{Hb} then consists of

$$T^{Hb} = \begin{bmatrix} \pi_1 & \pi_2 & \pi_3 \\ \pi_1 & \pi_2 & \pi_3 \\ \pi_1 & \pi_2 & \pi_3 \end{bmatrix}, \quad (7)$$

while the locally optimal transition matrix T^{Lo} is given by [17]

$$T^{Lo} = \begin{bmatrix} 0 & \frac{\pi_2}{1-\pi_1} & \frac{\pi_3}{1-\pi_1} \\ \frac{\pi_1}{1-\pi_1} & 0 & \frac{1-2\pi_1}{1-\pi_1} \\ \frac{\pi_1}{1-\pi_1} & \frac{\pi_2}{\pi_3} \frac{1-2\pi_1}{1-\pi_1} & 1 - \dots \end{bmatrix}. \quad (8)$$

The generalization of this matrix to the entire configuration space yields a sampling with the lowest possible error bars [23]. In practice this is impossible, and all we can hope for is that good sampling is achieved when applying this matrix to a local stochastic subprocess (which is here not independent of other subprocesses). A comparison between the heat-bath and locally optimal approach is made in Fig. 5 for a one-dimensional Bose-Hubbard model with parameters $U = 1, \mu = 0.5, \beta = 32, L = 32, V_{nn} = 0.4$ and varying tunneling amplitude t . The ratio of the standard deviation obtained by the locally optimal approach to the standard deviation obtained by the heat-bath approach is shown for the condensate fraction and the total energy. We see that the locally optimal approach is on average ten to fifteen percent better, but the effect is less pronounced than in the DLSSE [9, 10, 17, 20]. Even smaller differences were found for some other parameter regimes.

D. Scaling of the worm with system size

When using the worm and DLSSE methods, the needed computation time for a desired accuracy scales linearly with system size and inverse temperature. The scaling efficiency is further determined by the dynamical exponent z , which describes how the integrated autocorrelation time scales with system size and inverse temperature. The worm and directed loop algorithm have very low dynamical exponents; z is even zero in some high-dimensional cases. This beneficial scaling is the cornerstone for the study of very large system sizes at very low temperatures.

Since the present algorithm is based on the same principles as the directed loop algorithm and the worm algorithm, one expects that the dynamical exponent is similar (at least of the same order) but the prefactor of the scaling behavior might be different.

We studied the scaling behavior for the critical system of an isotropic spin-1/2 Heisenberg chain ($\Delta = J = 1$) in zero magnetic field ($H = 0$), for which the worm updates are fast. We investigated the effects of increasing system size L at fixed inverse temperature β on the one hand

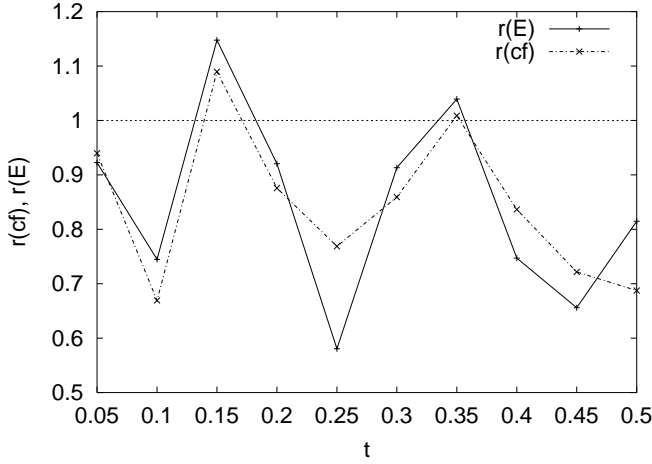


FIG. 5: Simulation of a one-dimensional Bose-Hubbard model with parameters $U = 1, \mu = 0.5, \beta = 32, L = 32, V_{nn} = 0.4$ and varying tunneling amplitude t . Plotted is the ratio r for the condensate fraction ($r(cf)$) and for the total energy ($r(E)$), being the ratio of the standard deviation σ_{Lo} obtained by the locally optimal approach to the standard deviation σ_{Hb} obtained by the heat-bath approach ($r = \frac{\sigma_{Hb}}{\sigma_{Lo}}$). Simulations consisted of 40 bins of 300 seconds on a Pentium III processor per data point.

and of increasing the inverse temperature β at fixed system size L on the other hand. This allows us to see whether the algorithm scales symmetrically with system size and temperature or not. All calculations ran for a fixed time of 40 bins of 300 seconds each on a Pentium III processor. We used optimal parameters for the simulation: we use the locally optimal transition matrix of eq.(8) and we set $E_{off} = 0.5$. We focused on the standard deviation and the integrated autocorrelation time of the kinetic energy, since the modes of this observable couple to the slowest mode of the simulation while the measurements can be calculated at low computational cost.

In Fig. 6 we study the standard deviation (statistical error) on the average kinetic energy per site. When the system size and the inverse temperature are sufficiently large, we see a gradual increase in the statistical error with an exponent of $\sigma \sim (L\beta)^{0.5}$, irrespective of whether L , β or both (note that the quantum imaginary time direction scales as one classical space direction) are increased. Since, for larger lattices, the worm will visit each site less often, this result is intuitively understandable. From the data in Fig. 6 we can already see that the dynamic exponent z obeys $0 < z \leq 1$. Strangely, when β is taken too low (see the data points at $L\beta = 16$ in Fig. 6), the present algorithm loses its efficiency. Below we will relate this to higher integrated autocorrelation times.

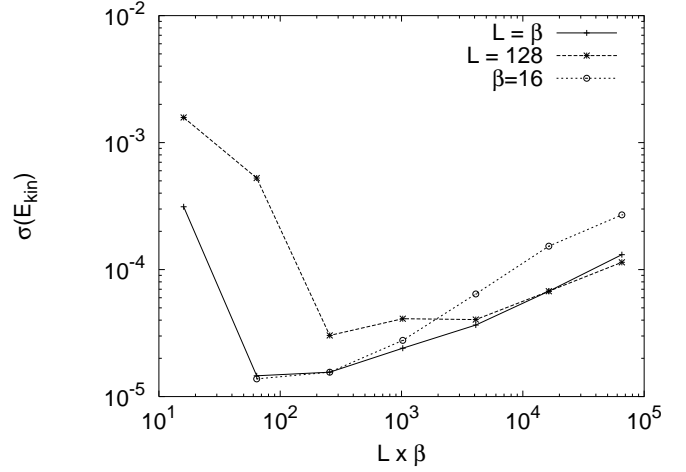


FIG. 6: Standard deviation on the average kinetic energy per site as a function of the system size L multiplied by the inverse temperature β for an isotropic spin-1/2 chain in zero magnetic field. Plots are shown when the system size and the inverse temperature are increased simultaneously ($L = \beta$), when the system size is held constant at $L = 128$ and only the temperature β is varied ($L = 129$), and when the temperature is held constant at $\beta = 16$ and the system size L varies ($\beta = 16$).

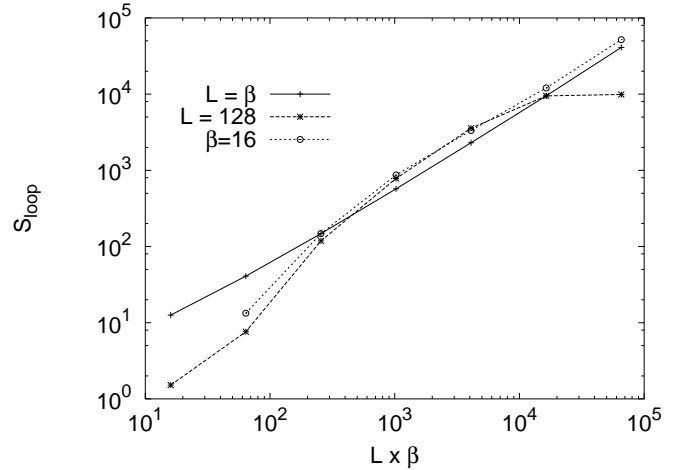


FIG. 7: Idem as in Fig. 6, but now the loop size (S_{loop}) is shown. The loop size S_{loop} is defined as the total number of interactions passed, inserted, annihilated and modified by the mobile worm in a single update.

A similar picture results when we look at the loop size in Fig. 7. We define the loop size S_{loop} as the total number of interactions passed, inserted, annihilated and modified by the mobile worm in a single update. We see that the loop size S_{loop} scales as $S_{loop} \approx (L\beta)^1$. The loop size increases thus linearly with the increase in area in space-time. However, if we are very close to the ground state at a fixed system size, then increasing β

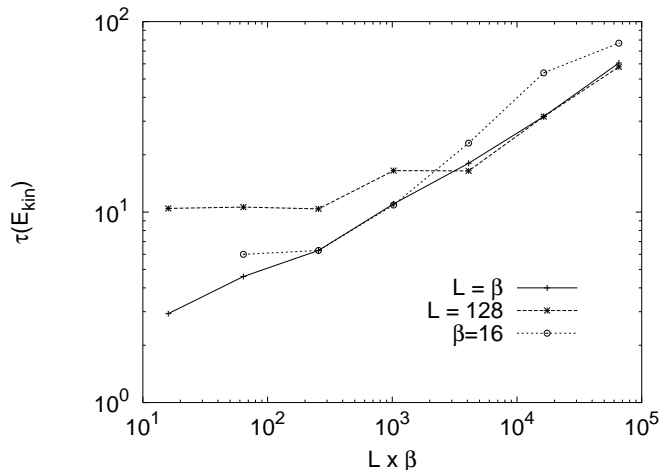


FIG. 8: Idem as in Fig. 6, but now the integrated autocorrelation time of the kinetic energy, $\tau(E_{kin})$ is shown.

does not result in longer loops and the algorithm loses its scaling properties.

The integrated autocorrelation time $\tau(E_{kin})$ of the kinetic energy in Fig. 8 shows a similar pattern: for large enough space-time areas, the integrated autocorrelation time scales as $\tau(E_{kin}) \sim (L\beta)^{0.42 \pm 2}$, where the exponent is again irrespective of whether L , β or both are increased. When the inverse temperature is too low, we unexpectedly find high autocorrelation times which explains the high standard deviations for the same data points in Fig. 6. This behavior could be due to the fact that the mobile worm is always forced to make relatively large jumps in the time direction.

With the DLSSE, the integrated autocorrelation time scales as $\tau(E_{kin}) \sim (L\beta)^{0.38 \pm 2}$. This result is in agreement with Ref. [9]. The dynamic exponent of the DLSSE is thus lower, yet in our calculations the standard deviations of the DLSSE increased more rapidly with increas-

ing system size. This is due to the increase in computational cost for a single update, which scales worse for the DLSSE. The computational cost of a single update depends strongly on the way of implementation, and the scaling of the standard deviations with system size should be interpreted accordingly. In addition, when looking at the magnetization on every site, the worm algorithm performs much better than the DLSSE for all system sizes. We conclude that efficiency largely depends on the implementation of the algorithm and on the observables of interest [20].

IV. CONCLUSION

In conclusion, we have presented a new formulation of the worm algorithm. The present algorithm has been derived using the concept of locally optimal Monte Carlo [17] and incorporates ideas both from the worm algorithm [7] and the directed loop algorithm [9] in the stochastic series expansion representation [8]. We have compared the efficiency of the present algorithm with that of the directed loop algorithm for spin chains and for the Bose-Hubbard chain. Especially when there are large diagonal matrix elements, the present worm algorithm is very successful. We have shown that choosing the locally optimal matrix for the transition matrices occurring in the stochastic subprocesses yields an efficient algorithm. We found that the loop size increases linearly with the increase in area in space-time, and that the dynamic exponent equals $z = 0.84 \pm 4$ for an isotropic Heisenberg chain without magnetic field. Seen the efficiency of the method and its advantageous scaling properties, the algorithm is suitable for large scale calculations of spin systems and of soft-core bosonic models.

The authors wish to thank the Research Board of the Universiteit Gent and the Fund for Scientific Research, Flanders for financial support. The authors acknowledge M. Troyer and S. Wessel for valuable discussions.

-
- [1] J. S. Liu, *Monte Carlo Strategies in Scientific Computing* (Springer Verlag, New York, USA, 2001).
 - [2] N. Metropolis, A. W. Rosenbluth, M. N. Metropolis, A. H. Teller and E. Teller, J. Chem. Phys. **21**, 1087 (1953).
 - [3] R. H. Swendsen and J. S. Wang, Phys. Rev. Lett. **58**, 86 (1987).
 - [4] U. Wolff, Phys. Rev. Lett. **62**, 361 (1989).
 - [5] D. Ceperley, Rev. Mod. Phys. **71**, S438 (1999).
 - [6] H. G. Evertz, G. Lana and M. Marcu, Phys. Rev. Lett. **70**, 875 (1993).
 - [7] N. V. Prokofev, B. V. Svistunov, and I. S. Tupitsyn, JETP Lett. **87**, 310 (1998).
 - [8] A. W. Sandvik, Phys. Rev. B **59**, 14157(R) (1999).
 - [9] O. F. Syljuåsen and A. W. Sandvik, Phys. Rev. E **66**, 046701 (2002).
 - [10] O. F. Syljuåsen, Phys. Rev. E **67**, 046701 (2003).
 - [11] N.V. Prokof'ev, B.V. Svistunov and I.S. Tupitsyn. JETP Lett. **64**, 911 (1996).
 - [12] M. Troyer, F. Alet, S. Trebst, and S. Wessel, AIP Conf. Proc. **690** (2003), see cond-mat/0306128.
 - [13] N. Kawashima and K. Harada, J. Phys. Soc. Jpn. **73**, 1379 (2004).
 - [14] S. M. A. Rombouts, K. Van Houcke, and L. Pollet, cond-mat/0508319 (2005).
 - [15] K. Van Houcke, S. M. A. Rombouts, and L. Pollet, cond-mat/0508431 (2005).
 - [16] W. K. Hastings, Biometrika **57**, 97 (1970).
 - [17] L. Pollet, S. M. A. Rombouts, K. Van Houcke and K.

- Heyde, Phys. Rev. E **70**, 056705 (2004).
- [18] L. Pollet, *PhD thesis*, Ghent University, Belgium, unpublished. see <http://inwpent4.ugent.be/PhDthesis.html> (2005).
- [19] S. Wessel, F. Alet, S. Trebst, D. Leumann, M. Troyer, and G. G. Batrouni, J. Phys. Soc. Jpn. Suppl. **74**, 10 (2005).
- [20] F. Alet, S. Wessel and M. Troyer, Phys. Rev. E **71**, 036706 (2005).
- [21] A. Dorneich and M. Troyer, Phys. Rev. E **64**, 066701 (2001).
- [22] P. H. Peskun, Biometrika **60**, 607 (1973).
- [23] A. Frigessi, C. R. Hwang and L. Younes, Ann. of Appl. Prob. **2**, 610 (1992).